International Journal of Nanoelectronics and Materials
IJNeaM
ISSN 1985-5761 | E-ISSN 2232-1535

Structural, Electrical and Piezoelectric Properties of $Ba_{1-x}Nd_xTiO_3$ Ceramic for Microelectronic Applications

Tuan Amirah Tuan Sulong[a,c,*], Rozana Aina Maulat Osman[a,c,*] Mohd Sobri Idris[b,c], Banu Poobalan[a], Nazuhusna Khalid[a], Wan Azlianawati Wan Aziz[a], Afzan Kamaruddin[a], Mohd Rosydi Zakaria[a], and Yasmin Abdul Wahab[d,*]

[a]*Faculty of Electronic Engineering & Technology, Universiti Malaysia Perlis, 02600 Arau, Perlis, Malaysia*
[b]*Faculty of Chemical Engineering & Technology, Universiti Malaysia Perlis, 02600 Arau, Perlis, Malaysia*
[c]*Centre of Excellence for Frontier Materials Research, Universiti Malaysia Perlis, 02600 Arau, Perlis, Malaysia*
[d]*Nanotechnology & Catalysis Research Centre, University of Malaya, 50603 Kuala Lumpur, Malaysia*
**Corresponding author. e-mail: rozana@unimap.edu.my, sobri@unimap.edu.my, yasminaw@um.edu.my*

Received 9 September 2025, Revised 9 October 2025, Accepted 27 October 2025

ABSTRACT

Neodymium (Nd)-doped barium titanate ($BaTiO_3$) ceramics with general formula $Ba_{1-x}Nd_xTiO_3$ ($0 \le x \le 0.13$) were synthesized by the conventional solid-state reaction method at 1400 °C for 36 hours in air. A single-phase structure of Nd-doped $BaTiO_3$ was observed from $0 \le x \le 0.10$. The tetragonal distortion of undoped $BaTiO_3$ progressively decreased with increasing Nd content (x). The samples retain a tetragonal structure for $x \le 0.015$, transformed to a cubic phase for $0.03 \le x \le 0.1$ and showed to coalesce at $x = 0.13$. The undoped $BaTiO_3$ exhibited a maximum permittivity approximately $\varepsilon = 8500$ at the Curie temperature (T_c), while a slightly reduced value of about $\varepsilon = 8200$ for Nd at $x = 0.005$. Nd substitution resulted in a shift of the permittivity maximum towards lower T_c within the tetragonal region, whereas compositions in the cubic displayed a nearly linear temperature dependence without a distinct maximum. The composition with $x = 0.005$ showed the highest piezoelectric charge coefficient, $d_{33} = 49$ pC/N and piezoelectric voltage coefficient of $g_{33} = 0.2 \times 10^{-2}$ V.m/N.

Keywords: *Neodymium doped barium titanate, Permittivity, Rietveld refinement, $BaTiO_3$*

1. INTRODUCTION

Researchers are attempting to reduce the size of all electronic devices to be as small and lightweight as possible. Due to this trend, high-permittivity materials such as barium titanate ($BaTiO_3$) have become increasingly important in ceramic materials. $BaTiO_3$, with its outstanding dielectric properties and high thermal stability, is widely used in the fabrication of electronic devices such as multilayer ceramic capacitors (MLCCs), positive temperature coefficient of resistance (PTCR) thermistors, piezoelectric sensors, transducers, and more [1–2].

$BaTiO_3$ exhibits a perovskite structure with the general formula ABO_3, can have its properties tailored through doping at either the A-site or B-site. Doping in $BaTiO_3$ is strongly influenced by the ionic radii of the dopant elements [3]. Recently, trivalent rare-earth elements have been reported as effective dopants to improve the physical and electrical properties of $BaTiO_3$ [4,5]. Morrison et al. [4], in his study, discovered an unusually high permittivity of approximately 25,000 in $BaTiO_3$ when doped with lanthanum (La) at both sites at high frequencies. This exceptionally high permittivity was accompanied by a trend of shifting the Curie temperature (T_c) to lower values. Due to its larger ionic radius, La appears to substitute exclusively at the A-site.

Neodymium (Nd) is another promising trivalent rare-earth element used as a dopant. The Nd^{3+} ion (1.27 Å) is presumed to occupy the Ba^{2+} site (1.61 Å) rather than the Ti^{4+} site (0.605 Å), due to size incompatibility. However, double substitution of Nd-doped $BaTiO_3$, as reported by Hirose et al. [5], resulted in structural changes from the tetragonal to cubic phase with increasing Nd content. In addition, the sharp maximum in permittivity broadens rapidly with increasing Nd and gradually shifts to lower temperatures. Nevertheless, there is limited information on the variation of lattice parameters, unit cell volume, complete structural refinement, and detailed electrical and piezoelectric properties of Nd-doped $BaTiO_3$.

Therefore, in this paper, a systematic study on the effect of Nd doping at the A-site in $BaTiO_3$ is presented. Rietveld refinement, as well as electrical and piezoelectric characterizations, are reported. The aim is to examine and, where necessary, optimize the electrical properties of sintered $BaTiO_3$ and Nd-doped $BaTiO_3$ for their potential in piezo electronic applications.

2. EXPERIMENTAL PROCEDURE

$Ba_{1-x}Nd_xTiO_3$ ceramics were synthesized via the conventional solid-state reaction method from high-purity commercial precursors: barium carbonate ($BaCO_3$) (99%), titanium dioxide (TiO_2) (99%), and neodymium (III) oxide (Nd_2O_3) (99%) obtained from Sigma-Aldrich. Stoichiometric amounts of the powders were weighed, thoroughly mixed in an agate mortar and pestle to ensure chemical homogeneity and then calcined in air at 1000 °C for 12 hours. The calcined powders were reground and uniaxially pressed into disc-shaped pellets (13 mm diameter, ~1 mm thickness) under a pressure of 5 tons. These pellets were sintered at 1400 °C for 6 hours in a programmable muffle furnace to achieve densification. Phase identification and structural analysis were performed using a Bruker D2 Phaser X-ray diffractometer equipped with a LYNXEYE 1D detector and Cu–Kα radiation. Data were collected at room temperature using a step size of 0.02° and a dwell time of 0.2 seconds. Rietveld refinements were conducted using the GSAS/EXPGUI software package[6-7], and crystallographic models were visualized with VESTA software [8], following refinement strategies from established literature [9-10]. The sintered pellets were polished and coated with silver paste to form electrodes, then fired to ensure proper electrical contact. Electrical property measurements, including dielectric properties, capacitance, and resistance, were carried out using an IM3570 HIOKI Impedance Analyzer over a frequency range of 10 Hz to 1 MHz and a temperature range of 40 °C to 200 °C, using a programmable furnace with a controlled heating rate of 5 °C/min.

3. RESULTS AND DISCUSSION

3.1. X-ray Diffraction Analysis

Figure 1(a) presents the X-ray diffraction (XRD) patterns of $Ba_{1-x}Nd_xTiO_3$ ceramics with varying Nd content ($0 \le x \le 0.13$). All compositions up to x = 0.10 exhibit a single-phase perovskite structure without detectable secondary phases, indicating successful incorporation of Nd^{3+} into the $BaTiO_3$ lattice. The diffraction pattern of undoped $BaTiO_3$ corresponds to a tetragonal structure with refined lattice parameters a = 3.9937 Å and c = 4.0342 Å, in close agreement with previously reported values (a = 3.994 Å, c = 4.038 Å) [11-12]. With Nd doping in the range of $0.03 \le x \le 0.10$, a structural transition from tetragonal to pseudo-cubic symmetry become observed. The characteristic peak splitting of the (002) and (200) reflections, indicative of tetragonality, gradually merges into a single peak as shown in the enlarged view in Figure 1(b). This behaviour suggests a progressive suppression of tetragonal distortion with increasing Nd concentration [13].

At low doping levels ($0 < x < 0.015$), a decrease in tetragonality is observed. The composition at x = 0.015 exhibits cubic symmetry with a lattice parameter of a = 4.0014 Å. As Nd content increases up to x = 0.10, the cubic structure is maintained and the lattice parameter increases linearly to 4.0050 Å. For $x \ge 0.13$, secondary phases begin to emerge, with additional diffraction peaks attributed to $Nd_2Ti_2O_7$ [13]. This indicates that the solubility limit of Nd in the $BaTiO_3$ lattice lies between x = 0.1 and 0.13. At x = 0.13, the primary phase remains cubic with a = 3.9995 Å, although the presence of impurity peaks confirms phase segregation beyond the solid solution limit.

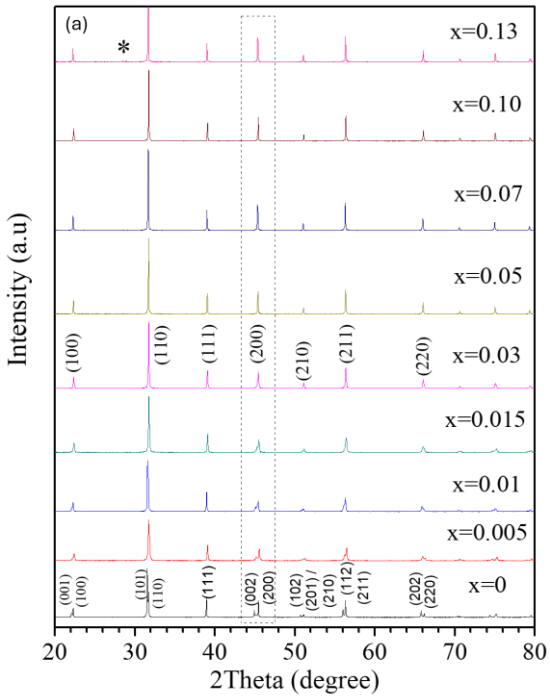

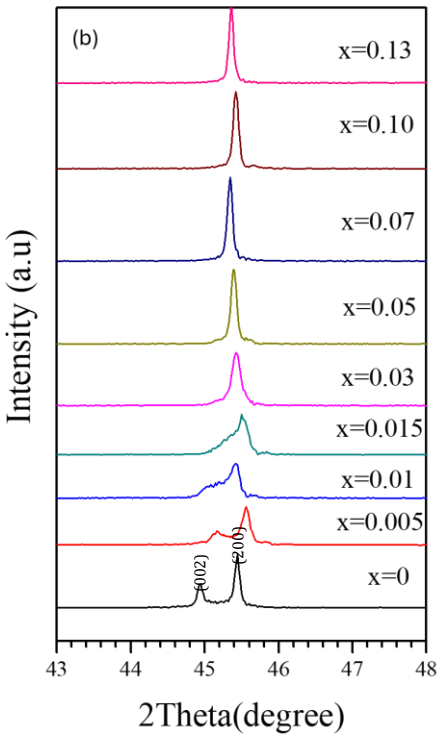

Figure 1. (a) XRD patterns of $Ba_{1-x}Nd_xTiO_3$ ceramics (b) Enlarge Xray Splitting XRD peak splitting for (002) and (200) reflection.

The evolution of lattice parameters as a function of Nd content is shown in Figure 2. For $0 \leq x \leq 0.015$, the lattice parameter an increase while c decreases slightly, resulting in a reduction in the c/a ratio and a corresponding decrease in unit cell volume. For $0.03 \leq x \leq 0.10$, the lattice parameter a remains nearly constant, consistent with a stable cubic phase. These variations are attributed to the substitution of smaller Nd^{3+} ions (1.27 Å) for larger Ba^{2+} ions (1.61 Å) at the A-site, leading to lattice contraction. The deviation from linearity in lattice parameters observed at $x \geq 0.13$ further supports the existence of a solubility limit. These results are consistent with those reported by Yao et al. [14].

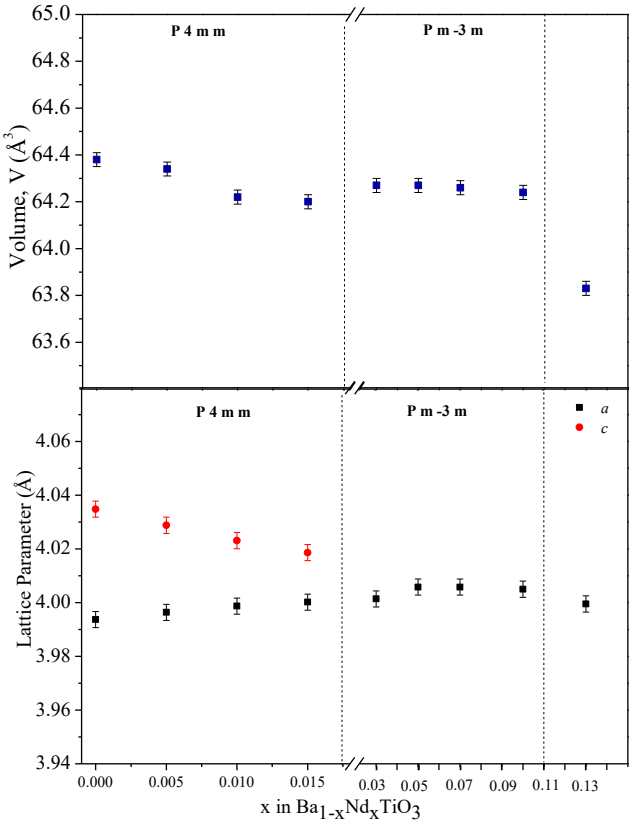

Figure 2. Lattice parameter and unit cell volume of $Ba_{1-x}Nd_xTiO_3$ ($0 \leq x \leq 0.13$).

In the refinement analysis, common parameters that can be refined include the scale factor, background, lattice parameters, 2θ zero, profile parameters, atomic positions, and thermal parameters, as reported elsewhere [9]. Table 1 presents the refinement data for tetragonal Nd-doped $BaTiO_3$. Small variations in the atomic positions of titanium and oxygen were observed, while the positions of barium and neodymium remained fixed. The substitution of Nd^{3+} creates Ba-site deficiencies to maintain charge neutrality, which increase with higher Nd content. Consequently, the tetragonal unit cell undergoes shrinkage, displacing the Ti^{4+} ions from the centre of the octahedral sites and weakening the TiO_6 octahedra. This structural distortion initiates a phase transition from tetragonal to cubic. Although the R-factors and χ^2 values are relatively higher than those of undoped $BaTiO_3$, they remain within acceptable limits.

Table 2 shows the R-factors (R_{wp} and R_p) for cubic Nd-doped $BaTiO_3$, which are considered acceptable and satisfactory (below 20%). Moreover, the χ^2 values are relatively low and below 5, indicating good fit quality [15]. The R_p and R_{wp} values confirm a reasonable agreement between the refined and observed XRD patterns for all $Ba_{1-x}Nd_xTiO_3$ ceramics, in both tetragonal and cubic phases. These results suggest that the structural refinement is reliable.

Table 1 Structural refinement data for Ba1-xNdxTiO3 ($0 \le x \le 0.015$)

Doping Concentration	x = 0.005	x = 0.01	x = 0.015
Ti, z	0.5169(8)	0.5142(1)	0.5136(1)
Ba (1a), U_{iso}	0.0076(3)	0.0058(3)	0.0069(3)
Nd (1a),U_{iso}	0.0139(2)	0.0169(2)	0.0059(2)
Ti (1b), U_{iso}	0.0080(1)	0.0069(1)	0.0057(1)
O1(1b), U_{iso}	0.0120(2)	0.0175(2)	0.0070(2)
O2(2c),U_{iso}	0.0010(2)	0.0095(4)	0.0142(2)
R_{wp} (%)	13.89	14.5	13.6
R_p (%)	11.04	13.1	10.5
χ^2	4.47	4.93	4.51

Table 2 Structural refinement data $Ba_{1-x}Nd_xTiO_3$ ($0.03 \le x \le 0.10$)

Doping Concentration	x = 0.05	x = 0.07	x = 0.10
Ti, z	-	-	-
Ba (1a), U_{iso}	0.0091(2)	0.007(2)	0.0072(2)
Nd (1a),U_{iso}	0.0075(2)	0.0069(2)	0.0174(2)
Ti (1b), U_{iso}	0.0079(2)	0.0051(2)	0.0054(2)
O1(1b), U_{iso}	0.0131(2)	0.0103(1)	0.0128(2)
O2(2c),U_{iso}	-	-	-
R_{wp} (%)	11.9	9.34	8.58
R_p (%)	9.04	7.24	4.99
χ^2	3.33	2.43	2.22

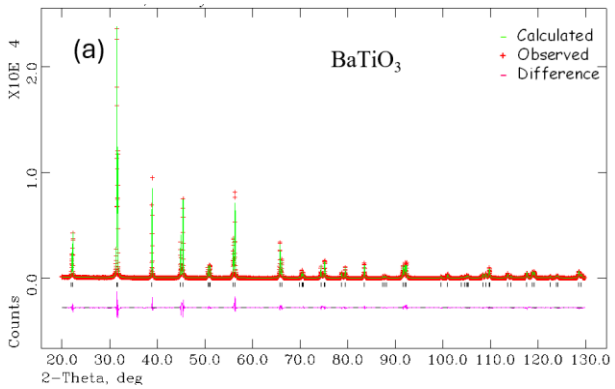

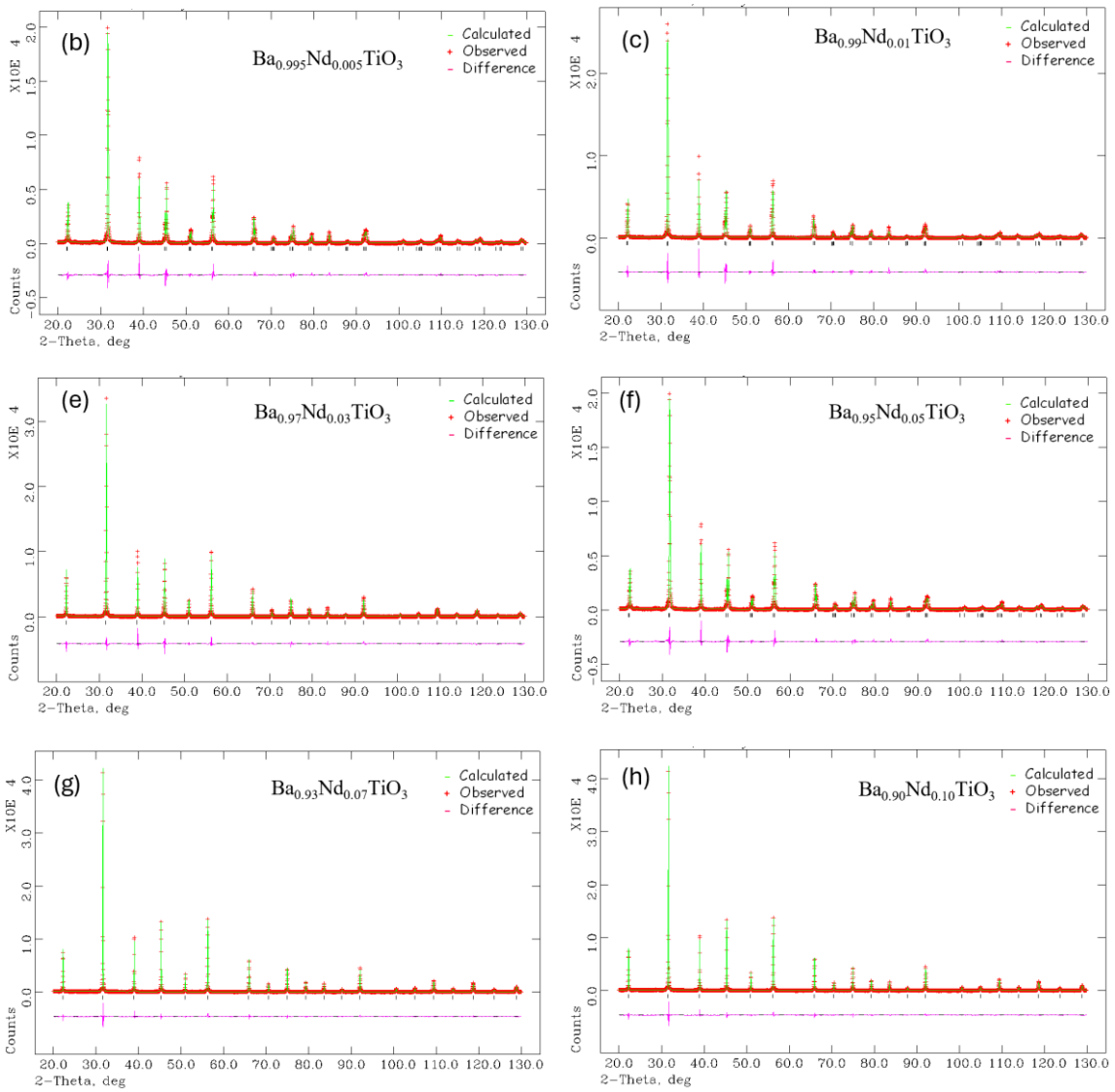

Figure 3. Plot of structural refinement of Ba1-xNdxTiO3 [a-h] (0 ≤ x ≤ 0.10).

The structural plot of Nd-doped $BaTiO_3$ in Figure 3 demonstrates good agreement between the experimental XRD patterns and the refined model.

3.2. Impedance Spectroscopy Analysis

Figure 4 (a-c) shows the variation in the maximum permittivity of Nd-doped $BaTiO_3$ ceramics as a function of temperature. Significant changes were observed upon addition of Nd^{3+}. The maximum permittivity sharp peak was lowered down with increasing Nd^{3+}. The decrease in permittivity was accompanied by a shift of T_c to lower temperature. The variation of permittivity with temperature shows a broadened maximum peak with increasing Nd^{3+} concentration. Undoped $BaTiO_3$ exhibited the highest permittivity, reaching approximately $\varepsilon \approx 8500$ at the Curie temperature (T_c) of 120 °C. However, with Nd doping ($0.005 \leq x \leq 0.015$), the maximum permittivity decreased to approximately 8200, 5800, and 2300, respectively, as measured at 1 kHz. The results show that the Nd^{3+} addition shifted the temperature of the maximal permittivity from 120 °C (x = 0) below than that for $0.03 < x < 0.10$. In contrast, samples with Nd content in the range $0.03 < x < 0.10$ exhibited nearly constant permittivity over the measured temperature range. The lower permittivity in the cubic region may be attributed to its location in the paraelectric region, where the material retains no residual polarization [16].

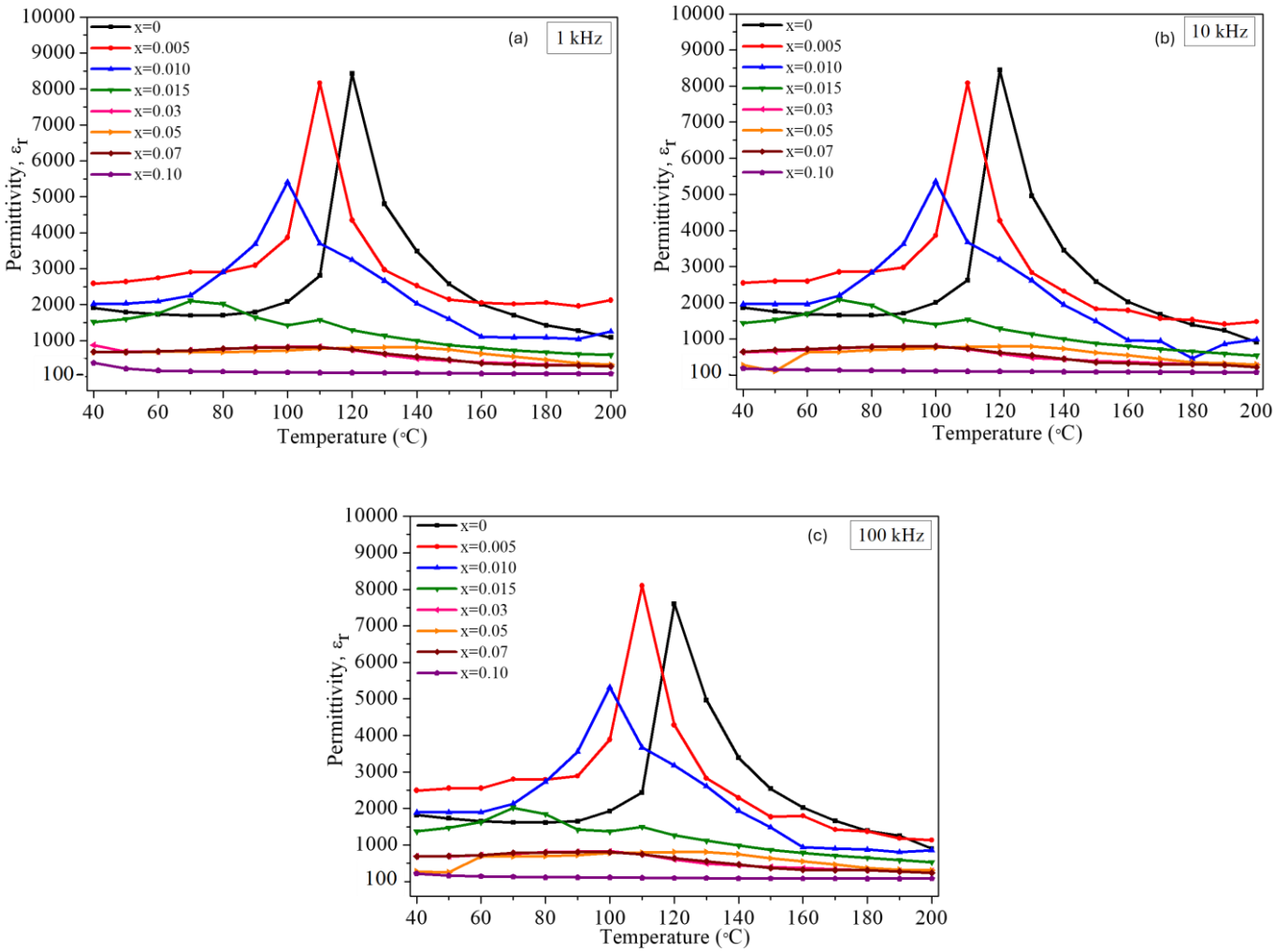

Figure 4. Permittivity of $Ba_{1-x}Nd_xTiO_3$ ($0 \le x \le 0.13$) at (a) 1 kHz (b) 10 kHz and (c) 100 kHz.

There was a decrease in permittivity with increasing frequency as shown in Figure 4. This trend also was previously observed by Ramirez [16], Yao et al., [14], Ganguly et al., [17], and Sharma et al. [18]. Permittivity value was slightly higher at low frequencies than at higher frequencies. At low frequencies, space charge polarization may become dominant contribution samples exhibiting very high permittivity, which is strongly related to dipole orientation, is unable to keep pace with rapidly varying electric field frequency. Thus, permittivity begins to decrease with increasing frequency due to the phase lag between dipole alignment and electric field [19].

Figure 5 shows the temperature dependence in dielectric loss of Nd-doped $BaTiO_3$ at three different frequencies. The dielectric loss of the $Ba_{1-x}Nd_xTiO_3$ is very low at much lower temperature remaining below 0.8 at 1 kHz. The dielectric loss is very low below Tc and increase slightly near Tc. However, the dielectric loss becomes very minimal as measured at frequency 10 kHz and 100 kHz. Dielectric loss of any material is related to the heat dissipated by the material, when electrical field is applied [20]. By doping with Nd, the dielectric loss of $BaTiO_3$ markedly drop to a lower value, from 0.10 to 0.004 at room temperature. This means that lower dielectric loss is preferable especially for device performance and efficiency.

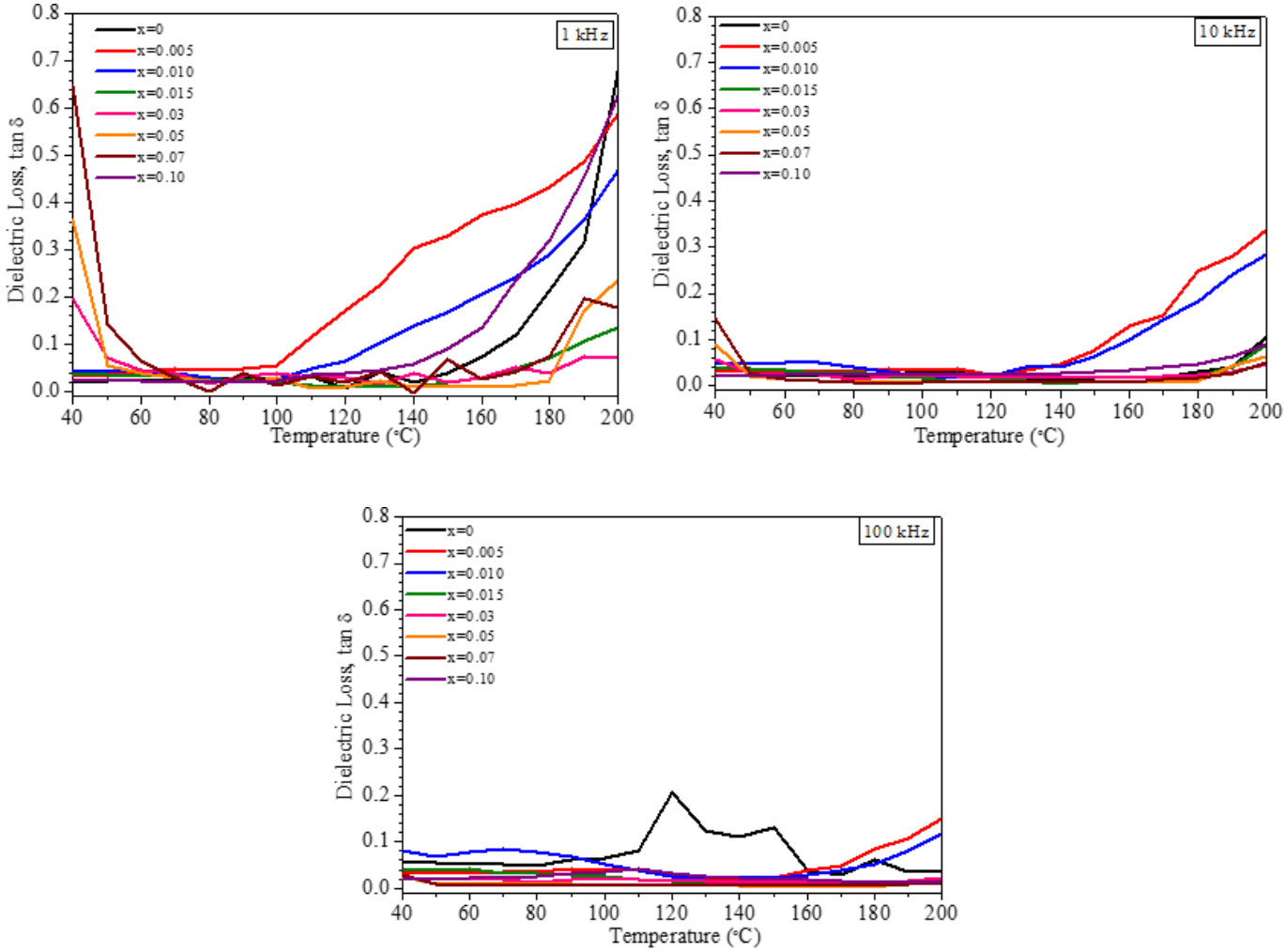

Figure 5. Dielectric loss of Ba1-xNdxTiO3 (0 ≤ x ≤ 0.13) at 1 kHz, 10 kHz and 100 kHz.

Figure 6(a) shows the frequency dependence conductivity of tetragonal Nd-doped $BaTiO_3$ and cubic Nd-doped $BaTiO_3$ in Figure 6(b) across frequency of 1 kHz to 100 kHz. Log σ versus log frequency below 1 kHz were excluded, as it essentially shows noisy data since sample impedance lies outside the measuring range of instrumentation [21]. For pure $BaTiO_3$, the linear region of log σ at 10 Hz to 1 kHz belonged to DC conductivity (which was excluded from extracted frequency due to noisy data. Above 1 kHz, log σ was the essence of the AC conductivity. The conductivity of $BaTiO_3$ increased linearly with the frequencies from 1 kHz to 100 kHz. Overall conductivity of tetragonal Nd-doped $BaTiO_3$ lies in the range of 10^{-5} to 10^{-8} Scm^{-1}. The addition of x seemed to influence the original conductivity of pure $BaTiO_3$. Sample Nd-doped $BaTiO_3$ ($0.3 \leq x \leq 0.10$) showed the conductivity of typical insulator [15] which at lower temperature, the conductivity lies in range of 10^{-8} to 10^{-7} Scm^{-1}. However, it shows the gradual increment with increasing temperatures. Therefore, total conductivity was affected by temperatures and frequencies.

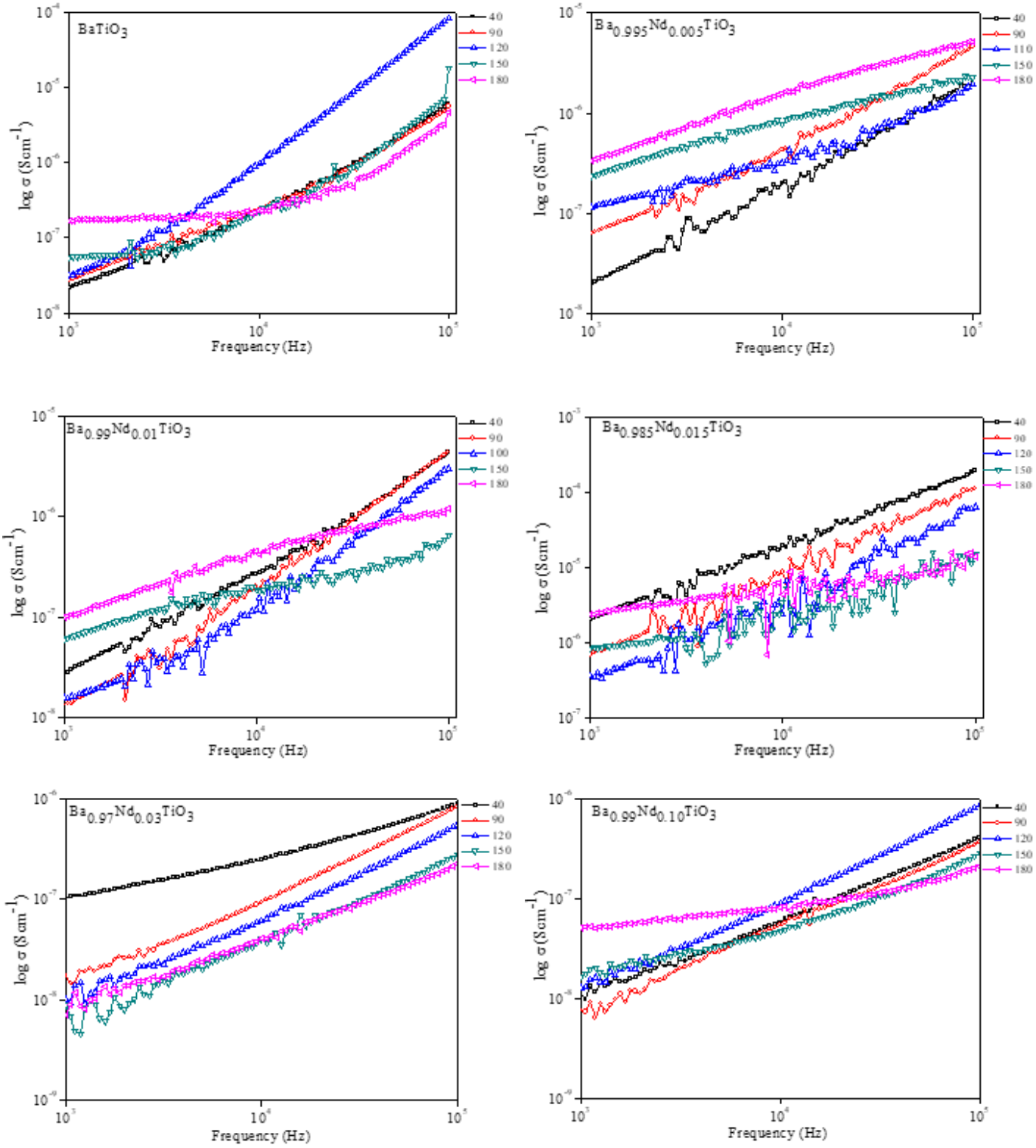

Figure 6. Conductivity of $Ba_{1-x}Nd_xTiO_3$ ($0 \leq x \leq 0.13$) at 1 kHz, 10 kHz and 100 kHz.

The piezoelectric charge constant (d_{33}) as a function of Nd addition is shown in Figure 7. With increasing Nd content (x), the d_{33} value decreases. However, for each sample, d_{33} increases with higher poling voltage. The reduction in d_{33} correlates with the decrease in permittivity upon Nd addition. The application of high poling voltage enhances the piezoelectric effect, likely due to improved domain alignment during the poling process in $BaTiO_3$ ceramics. It is presumed that the addition of Nd reduces the number of domains that align during poling as reported by Ganguly et al [17]. Furthermore, the structural transition from the tetragonal to cubic phase weakens the ferroelectricity of the samples. Although high d_{33} is partly attributed to high permittivity, the Nd-doped $BaTiO_3$ samples ($0.005 \leq x \leq 0.015$) exhibit lower d_{33} values. This may be due to the large strain observed in the grains of Nd-doped $BaTiO_3$, which also contributes to the reduced d_{33} values [17].

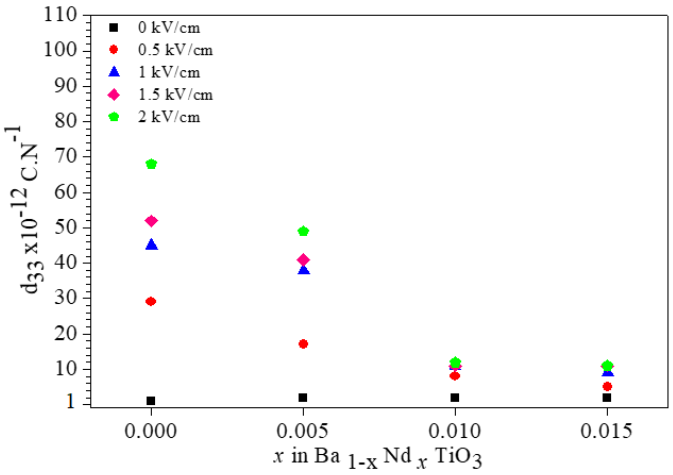

Figure 7. Piezoelectric charge constant, d_{33} of $Ba_{1-x}Nd_xTiO_3$ ($0 \le x \le 0.015$) in varied poling voltage.

Figure 8 shows the piezoelectric voltage constant (g_{33}) of Nd-doped $BaTiO_3$ as a function of poling voltage. At a maximum poling electric field of 2 kV/cm, the g_{33} value increased significantly, reaching 7×10^{-2} V·m/N, 1×10^{-2} V·m/N, 0.7×10^{-2} V·m/N, and 0.5×10^{-2} V·m/N for various Nd concentrations. The piezoelectric voltage constant, g_{33}, of both undoped and Nd-doped $BaTiO_3$ shows a notable decrease in parallel with the d_{33} values. This strongly suggests that both poling electric field and poling temperature significantly influence the g_{33} values, in addition to the intrinsic properties of the material.

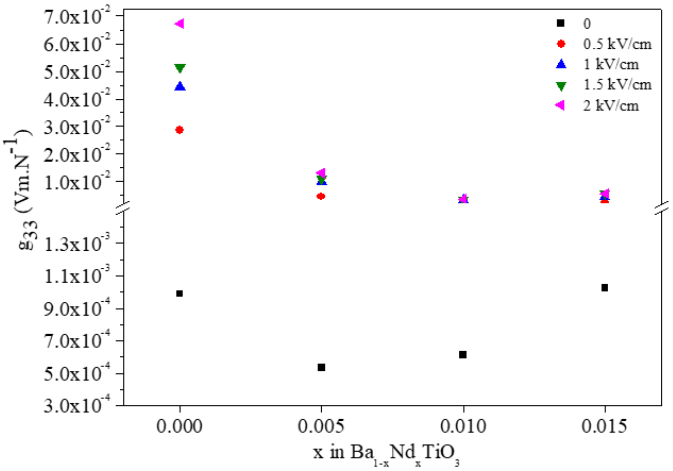

Figure 8. Piezoelectric voltage constant, g_{33} of $Ba_{1-x}Nd_xTiO_3$ ($0 \le x \le 0.015$) in varied poling voltage.

4. CONCLUSION

The modification of structural, electrical, and piezoelectric properties of neodymium-doped $BaTiO_3$ is attributed to the incorporation of Nd^{3+} ions into the Ba^{2+} sites. At low doping levels (small x), the tetragonal structure is retained in the XRD patterns, though accompanied by a reduction in lattice parameters and unit cell volume. Further increases in Nd content leads to the creation of Ba-site vacancies, which in turn initiate a structural transition from tetragonal to cubic. The solid solution range was determined to be $0 \le x \le 0.10$. Rietveld refinement was employed to model the [$BaTiO_3$], [Nd_2O_3], and [TiO_6] units within the crystal lattice. The refinement results showed relatively low χ^2 values and acceptable R-factors (below 20%). The Ti atom positions tend to shift toward the center of the octahedron due to the reduction in tetragonality associated with Nd^{3+} substitution for Ba^{2+}.

Electrical characterization revealed that neodymium doping significantly lowered the Curie temperature (Tc) to below 30 °C. This shift in Tc is consistent with the observed decrease in permittivity as x increases. Neodymium also inhibits the formation of ferroelectric domains, suppressing the alignment of individual dipoles. Conductivity analysis showed that $\log \sigma$ exhibited both frequency and temperature dependence within the range $0 \le x \le 0.015$. The piezoelectric properties (such as d_{33}) also decreased significantly with increasing Nd content, likely due to reduced remanent polarization after the poling process. These findings strongly highlight the critical role of doping mechanisms in generating structural defects that alter the fundamental properties of pure $BaTiO_3$.

ACKNOWLEDGMENTS

The authors acknowledge the financial support from the Ministry of Education, Malaysia for funding this project (FRGS Grant No: 9003-00496). The authors are also grateful for the excellent technical support from the Thin-Film Nanomaterials Research Group, School of Applied Physics, Faculty of Science and Technology, Universiti Kebangsaan Malaysia for the measurement of piezoelectric properties.

REFERENCES

[1] IS. Gablenz, C. Damm, F.W Muller, G. Israel, M. Rossel, A. Roder, H. P. Abicht. (2001). Preparation and Characterization of Core-Shell Structured TiO_2-$BaCO_3$ Particles. Solid State Sciences, 3, 291–299.

[2] P. Phule and S. H. Risbud. (1990). Review: Low-Temperature Synthesis and Processing of Electronic Materials in The BaO–TiO_2 System. Journal of Materials Science, 25, 1169–1183.

[3] R. D. Shannon and C. T. Prewitt, (1970), Revised Value of Effective Ionic Radii, Acta Crystallography, 2, 26, 1046-1048.

[4] F. D. Morrison, D. C. Sinclair, and A. R. West, (1999), Electrical and Structural Characteristics of Lanthanum-doped Barium Titanate Ceramics, Journal of Applied Physics, 86, 11, 6355-6366.

[5] N. Hirose, J. M. S. Skakle & A. R. West. (1999). Doping Mechanism and Permittivity Correlations in Nd-Doped $BaTiO_3$, Journal of Electroceramics, 3, 3, 233-238.

[6] A. C. Larson and R. B. V. Dreele. (1994). General Structure Analysis System (GSAS), Los Alamos National Laboratory Report LAUR, 86-748.

[7] L. B. McCusker, R. B. Von Dreele, D. E. Cox, D. Louer, D., and P. Scardi, (1999), Rietveld Refinement Guidelines, Journal of Applied Crystallography, 32, 36-50.

[8] K. Momma and S. Izumi, (2010), VESTA: a Three-Dimensional Visualization System for Electronic and Structural Analysis, 1-156.

[9] M. S. Idris, and R. A. M. Osman, (2013), Structure Refinement Strategy of Li-based Complex Oxides Using GSAS-EXPGUI Software Package, Advanced Materials Research, 795, 479-482.

[10] B. H. Toby, (2006). R factors in Rietveld Analysis: How Good is Good Enough?, Powder Diffraction, 2, 67-70.

[11] H. T. Evans, Jr, (1961), An X-Ray Diffraction Study of Tetragonal Barium Titanate, Acta Crystallography, 14, 1019-1026.

[12] S. Miyake & R. Ueda, (1947), On Phase Transformation of $BaTiO_3$, Journal of Physics Society, 2, p. 93.

[13] J. G. Pepin, E. R. Vance & G. J. McCarthy, (1981), Subsolidus Phase Relations in the System CeO_2-RE_2O_3 (RE_2O_3=C-type Rare Earth Sesquioxide), Journal of Solid-State Chemistry, 38, pp. 360-367.

[14] Z. Yao, H. Liu and Z. Y. Liu. (2008). Structure and Dielectric Behavior of Nd-doped $BaTiO_3$ Perovskites. Materials Chemistry and Physics, 109, 475–481.

[15] A. R. West. (2014). Basic Solid-State Chemistry, 2nd edition. Chichester: John & Wiley & Sons Ltd.

[16] R. F. Ramirez, A. Huanosta, E. Amano, R. Valenzuela, and A. R. West, (1989), Curie-Weiss Behavior in Polycrystalline Barium Titanate from AC Measurements, Ferroelectrics, 99:1, 195-201.

[17] M. Ganguly, S. K. Rout, P. K. Barhai, C. W. Ahn, and I. W. Kim. (2013). Structural, Electrical and Optical Properties of $Ba_{1-x}Nd_{2x/3}TiO_3$ Ceramics, Phase Transitions, 1-18.

[18] S. Sharma, K. Shamim, A. Ranjan, R. Raib, P. Kumari, and S. Sinha, (2015), Impedance and Modulus Spectroscopy Characterization of Lead-Free Barium Titanate Ferroelectric Ceramics, Ceramics International,41, 7713–7722.

[19] Keysight Literature Number 5980-2862EN, (2008), Solutions for Measuring Permittivity and Permeability with LCR Meters and Impedance Analyzers.

[20] S. T. Mailadil, R. Ubic, and H. Jantunen, (2017), Microwave Materials and Applications: Volume 1, John & Wiley & Sons Ltd., Chapter 2, 73.

[21] M. A. Hernandez, N. Maso, and A. R. West. (2016). On the Correct Choice of Equivalent Circuit for Fitting Bulk Impedance Data of Ionic/Electronic Conductors, Applied Physics Letters, 108, 152901, 1-5.